Some Effects Near Transition

E. Métral
CERN, Geneva, Switzerland

Abstract
This paper discusses some general longitudinal and transverse beam dynamics effects that occur near the transition energy and when it is crossed, with application to the particular cases of the CERN Proton Synchrotron and Super Proton Synchrotron machines.

Keywords
Transition energy; transition crossing; non-adiabatic motion; quadrupolar oscillation; transverse instability; gamma transition.

1 Transition energy

The momentum compaction factor α_p is a parameter which arises from the accelerator lattice (i.e., the transverse beam optics) and plays a major role in the longitudinal beam dynamics. It is given by [1, 2]

$$\alpha_p = \frac{\mathrm{d}C/C}{\mathrm{d}p/p} = \frac{1}{C}\int_0^C \frac{D_x(s)}{\rho(s)}\,\mathrm{d}s\,, \tag{1}$$

where C is the circumference of the machine (the length of the particle trajectory), p is the beam momentum, D_x is the horizontal dispersion, ρ is the bending radius, and s is the azimuthal coordinate around the machine. For most circular machines $\alpha_p > 0$, and the relativistic mass factor at transition (called 'gamma transition' and written γ_t) is given by [2]

$$\gamma_t = \frac{1}{\sqrt{\alpha_p}}. \tag{2}$$

However, $\alpha_p < 0$ is also possible (e.g., as in the LEAR machine at CERN in the past [3]), in which case the lattice is called a Negative Momentum Compaction (NMC) lattice or imaginary-γ_t lattice. Assuming a positive momentum compaction factor, it can be deduced from Eq. (1) that an increase in the beam momentum leads to an increase in the circumference. However, an increase in the beam momentum also leads to an increase in the beam velocity. Depending on the beam energy, the increase in the circumference may be either larger or smaller than the increase in the beam velocity, and the revolution frequency may either decrease or increase. At very high energy, the beam velocity is close to the velocity of light (c) and remains about constant, which leads to a decrease in the revolution frequency. At low energy, the beam velocity increases faster than the circumference and the revolution frequency increases. There is an energy at which the velocity variation is compensated by the circumference variation, i.e., $\mathrm{d}f_{\mathrm{rev}} = 0$ (where f_{rev} is the revolution frequency), and this energy is called the transition energy.

In fact, the important parameter for the longitudinal beam dynamics is the slip factor η, which is a measure of the distance from the transition energy and is given by [2]

https://doi.org/10.23730/CYRSP-2017-003.213

$$\eta = -\frac{\mathrm{d}f_{\mathrm{rev}} / f_{\mathrm{rev}}}{\mathrm{d}p / p} = \alpha_{\mathrm{p}} - \frac{1}{\gamma^2} = \frac{1}{\gamma_{\mathrm{t}}^2} - \frac{1}{\gamma^2}, \tag{3}$$

where γ is the relativistic mass factor of the beam. The slip factor is negative below transition, equal to zero at transition (this is called the isochronous condition), and positive above transition.

2 Longitudinal beam dynamics 'far' below or above transition

This is the usual (classical or adiabatic) case. The bucket separatrices are recalled in Fig. 1 for several values of the synchronous phase ϕ_{s} below and above transition [2], using the RF phase ϕ and its time derivative (a dot denotes the derivative with respect to time) as variables, where Ω_{s} is the angular synchrotron frequency, given by

$$\Omega_{\mathrm{s}} = \Omega_{\mathrm{rev}} \sqrt{-\frac{eV_{\mathrm{RF,peak}}\, h\eta \cos\phi_{\mathrm{s}}}{2\pi\beta^2 E_{\mathrm{total}}}}\ . \tag{4}$$

Here, Ω_{rev} is the angular frequency of revolution, e is the elementary charge, $V_{\mathrm{RF,peak}}$ is the peak RF voltage, h is the RF harmonic number, β is the relativistic velocity factor, and E_{total} is the total beam energy. As the term under the square root sign in Eq. (4) has to be positive (for stable particle motion), the synchronous phase ϕ_{s} has to be shifted to $\pi - \phi_{\mathrm{s}}$ above transition. Some examples of particle trajectories are shown in Fig. 2.

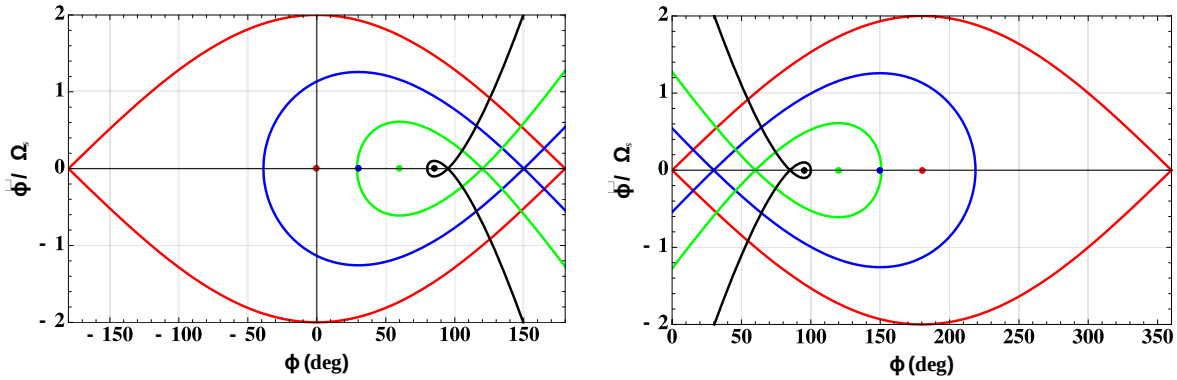

Fig. 1: RF bucket separatrices. Left, below transition for several synchronous phases: 0° (red), 30° (blue), 60° (green), 85° (black). Right, above transition for several synchronous phases: 180° (red), 150° (blue), 120° (green), 95° (black).

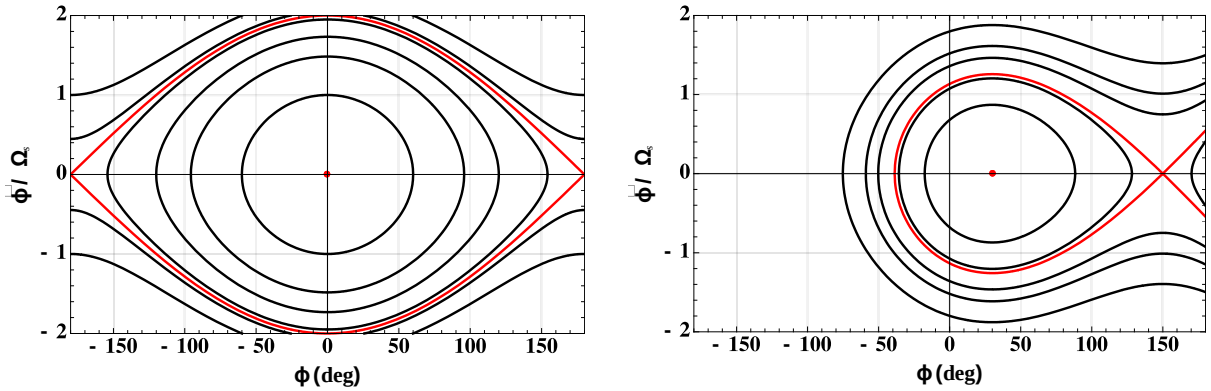

Fig. 2: Examples of particle trajectories (black) below transition, inside and outside the bucket separatrices (red), for two synchronous phases: 0° (left) and 30° (right).

3 Transition crossing

The case 'far' below or above transition discussed in Section 2 corresponds to the case where the adiabaticity condition

$$\frac{1}{\Omega_s^2}\left|\frac{d\Omega_s}{dt}\right| \ll 1 \tag{5}$$

is satisfied. 'Close' to transition, the adiabaticity condition is not satisfied any more and a non-adiabatic description of the synchrotron motion is necessary, as the particles will not be able to catch up with the rapid modification of the bucket shape [1, 4]. To describe the synchrotron motion close to transition, a non-adiabatic (characteristic) time T_c is defined by

$$T_c = \left(\frac{\beta^2 E_{rest} \gamma_t^4}{4\pi f_{rev}^2 \dot{\gamma} h V_{RF,peak} \left|\cos\phi_s\right|} \right)^{1/3}, \tag{6}$$

where E_{rest} is the beam rest energy. In the particular case of the bunch used for the nTOF facility [5] in the CERN Proton Synchrotron (PS), whose main parameters are reported in Table 1, the non-adiabatic time is ~2 ms.

Table 1: Relevant parameters for the CERN PS and the nTOF bunch [5]

Parameter	**Symbol (units)**	**Value**
Average machine radius	R (m)	100
Bending dipole radius	ρ (m)	70
Variation of the magnetic field	dB/dt (T/s)	2.2
Peak RF voltage	$V_{RF,peak}$ (kV)	200
RF harmonic number	h	8
Momentum compaction factor (gamma transition)	α_p (γ_t)	0.027 (6.1)
Longitudinal (total) emittance	ε_L (eV s)	2
Number of protons/bunch	N_b (10^{10} p/b)	800
Normalized r.m.s. transverse emittance	$\varepsilon^*_{x,y}$ (μm)	5
Transverse average betatron function	$\beta_{x,y}$ (m)	16
Beam pipe half-gaps	$b_{x,y}$ (cm)	3.5, 7.0
Transverse tunes	$Q_{x,y}$	6.25

The general variation of the bunch length, normalized by the value at transition, and of the momentum spread, obtained using a non-adiabatic theory (neglecting intensity effects for the moment), is depicted in Fig. 3, where several interesting features can be observed. First, contrary to the adiabatic theory, the bunch length does not decrease to zero at transition but reaches a minimum value. Second, the values of the bunch length and momentum spread below and above transition are symmetric with respect to the transition. Third, the product of the bunch length and the momentum spread is not constant, which means that the particle trajectory (which is an ellipse for small synchrotron amplitudes) is not always upright. The variation of the angle of the tilted ellipse around transition is shown on the left in Fig. 4, and the shape of the ellipse (using time and energy as variables) at transition is shown on the right.

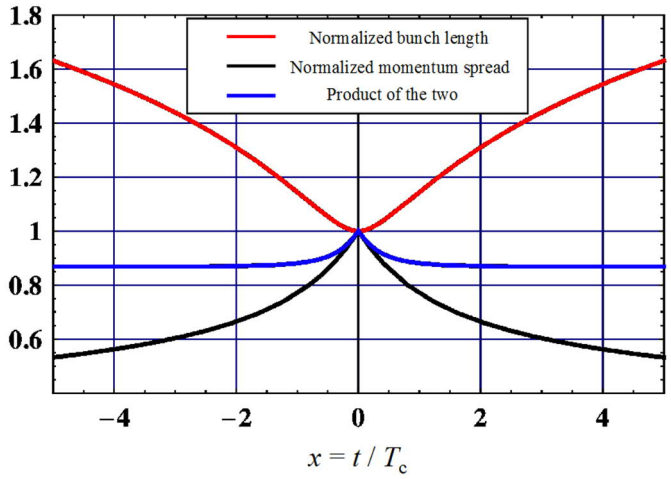

Fig. 3: General variation of the bunch length (normalized by the value at transition) and momentum spread close to transition obtained using the non-adiabatic theory [1, 4].

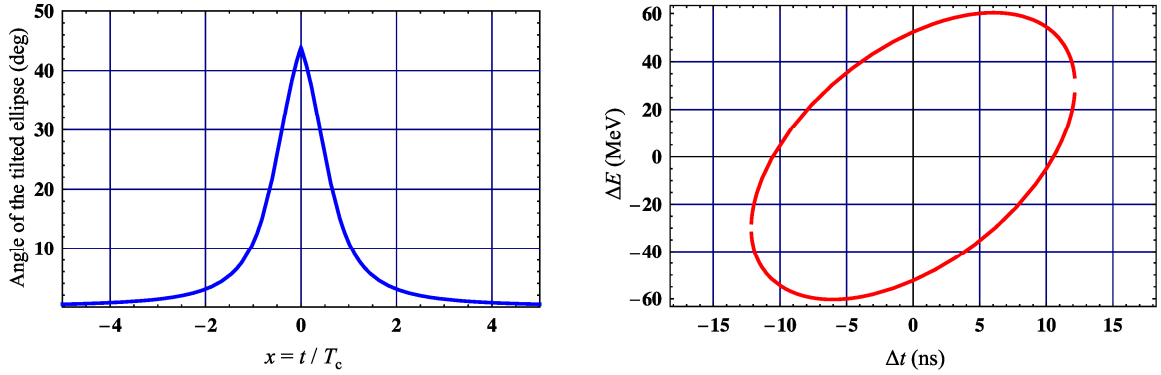

Fig. 4: Left, variation of the angle of the tilted ellipse (particle trajectory for small synchrotron amplitudes) around transition. Right, shape of the ellipse at transition.

As the bunch intensity increases, the effects of intensity (such as the longitudinal space charge effect and the interaction with the longitudinal impedance) cannot be neglected any more [4, 6, 7]. Considering first only the longitudinal space charge effect, as it is defocusing below transition, the final bunch length below transition will be longer than predicted above. Furthermore, as the longitudinal space charge effect is focusing above transition, the final bunch length above transition will be shorter than predicted above. This means that, because of the longitudinal space charge effect, an intensity-dependent step (i.e., a longitudinal mismatch) will thus appear at transition, as can be seen in Fig. 5 for the static case (i.e., when the transition is not crossed). In the dynamic case (i.e., when the transition is crossed), because of the longitudinal mismatch introduced by the intensity-dependent step at transition, the bunch length will oscillate, as can be seen in Fig. 6. Considering now, instead of the longitudinal space charge effect, the interaction with the inductive part of the longitudinal broadband impedance, the situation is similar but the bunch length is shorter below (and larger above) transition owing to the focusing (or defocusing) effect of the impedance (see Fig. 7). Detailed measurements (which can be used to estimate the imaginary part of the longitudinal impedance) on the CERN PS can be found in Ref. [8].

There are two main remedies for overcoming these intensity effects (and some other remedies, which will also be discussed below):

– Avoid crossing the transition in the design phase, i.e., use $\alpha_p < 0$.

– If transition crossing cannot be avoided, use a 'γ_t jump', which consists in an artificial increase in the transition-crossing speed by means of fast pulsed quadrupoles (at locations of non-zero dispersion) [1].

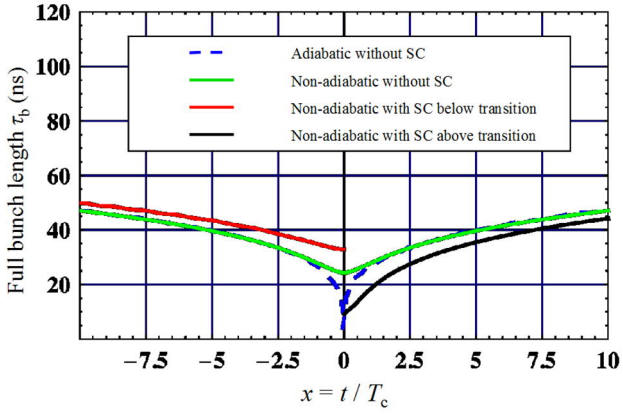

Fig. 5: Evolution of the full (4σ) bunch length versus time near transition (occurring at time 0) in the case of the adiabatic theory without Space Charge (SC), and in the case of the non-adiabatic theory with and without SC in the static case (i.e., without crossing the transition), applied to the CERN PS nTOF bunch (see Table 1).

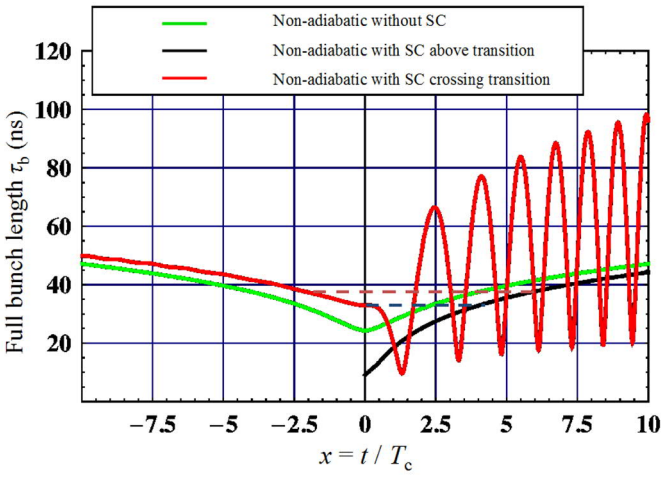

Fig. 6: Evolution of the full (4σ) bunch length versus time near transition (occurring at time 0) in the case of the non-adiabatic theory with and without space charge in the dynamic case (i.e., crossing the transition), applied to the CERN PS nTOF bunch (see Table 1).

The γ_t jump in the PS is shown in Fig. 8, where the effective crossing speed is increased by a factor ~50. As can be seen from Fig. 6, the idea of the γ_t jump is to switch, as fast as possible, from a certain bunch length below transition to the same bunch length above transition to avoid longitudinal quadrupolar oscillations (which ultimately lead to longitudinal-emittance blow-up through filamentation). One possibility could be to start the γ_t jump exactly at transition (see the dashed blue line in Fig. 6), which would lead to the smallest jump, but in this case we would move from a tilted to a non-tilted ellipse (see Fig. 4), which would still lead to some mismatch. It is cleaner to start the γ_t jump earlier, say at $\sim -2T_c$ (see Fig. 6), to avoid the effect of the tilted ellipse; this leads to a larger jump (see the dashed brown line in Fig. 6). In both cases, owing to the asymmetry introduced by intensity effects below and above transition, the optimum γ_t jump is asymmetric.

As discussed above, the important parameter for the longitudinal beam dynamics is the slip factor η, whose variation around transition is shown in Fig. 9. As can be seen, in the presence of the γ_t jump, the absolute value of the slip factor is kept above a certain value (which has to be defined

depending on the machine parameters and the issues observed) for most of the time, except for a very short time (~500 μs) close to transition.

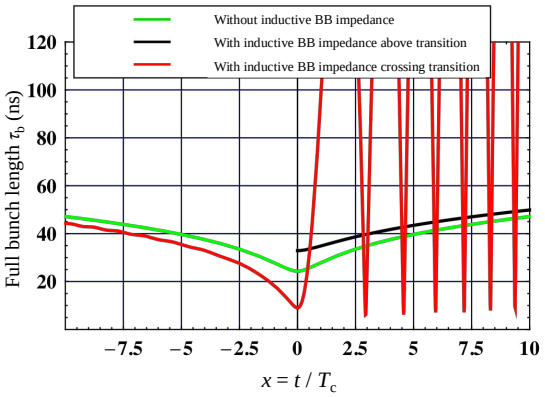

Fig. 7: Evolution of the full (4σ) bunch length versus time near transition (occurring at time 0) in the case of the non-adiabatic theory with (only) and without an inductive broadband (BB) impedance in the dynamic case (i.e., crossing the transition), applied to the CERN PS nTOF bunch (see Table 1). Here, a broadband impedance with an inductive part of 20 Ω has been used.

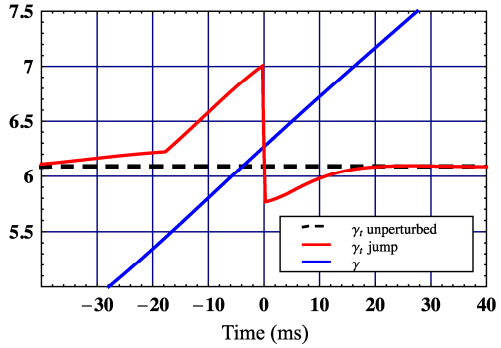

Fig. 8: Evolution of the relativistic mass factor γ (with $\mathrm{d}\gamma/\mathrm{d}t = 49.9\ \mathrm{s}^{-1}$) for the CERN PS nTOF bunch (see Table 1) around transition (occurring at time 0) and of γ_t, without (i.e., unperturbed) and with a jump.

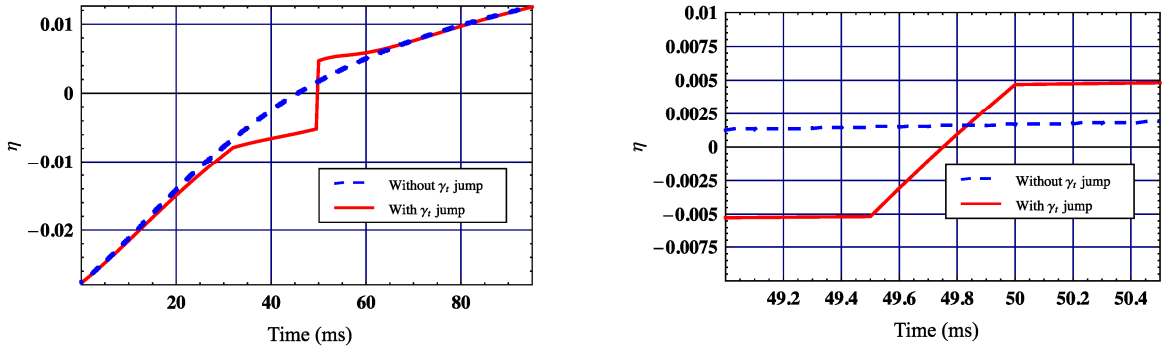

Fig. 9: Left, evolution of the slip factor η around transition (corresponding to Fig. 8) without and with the γ_t jump. Right, zoom close to transition, which reveals that the absolute value of the slip factor is 'small' for only a very short time (~500 μs).

4 Transverse (slow) head–tail instability

If the sign of the chromaticities (which are of order −1 for an uncorrected machine such as the CERN PS) is not changed (in both transverse planes) above transition, a (single-bunch) head–tail instability

may develop. This occurs only above a certain intensity in practice, even though this kind of instability has no threshold, owing to its rise time and to intrinsic non-linearities, which provide some Landau damping. This (slow) instability can be damped through Landau damping [6] using octupoles, which introduce some amplitude detunings. This method was used in the past to stabilize the PS beam. However, the better method of changing the sign of the chromaticities (and keeping them at small positive values) by acting on the optics with sextupoles was then adopted, and this has been a routine operation at the PS for many years. The transverse chromatic frequencies should be (slightly) positive to prevent the head–tail mode 0 (the most critical) from developing [1]:

$$f_{\xi_{x,y}} = Q_{x,y} f_{\mathrm{rev}} \frac{\xi_{x,y}}{\eta} > 0 \,, \tag{7}$$

where $\xi_{x,y}$ are the transverse chromaticities. An example of a transverse head–tail instability observed in the PS at injection (below transition) is shown in Fig. 10 (top), where several consecutive traces from a pick-up are superimposed and a clear ‘standing-wave’ pattern (with four nodes, called ‘mode 4’) can be observed. A comparison with an analytical prediction (for a bunch passing through the centre of the pick-up) is shown in Fig. 10 (bottom). The difference is mainly due to the fact that the measured bunch did not pass through the centre of the pick-up.

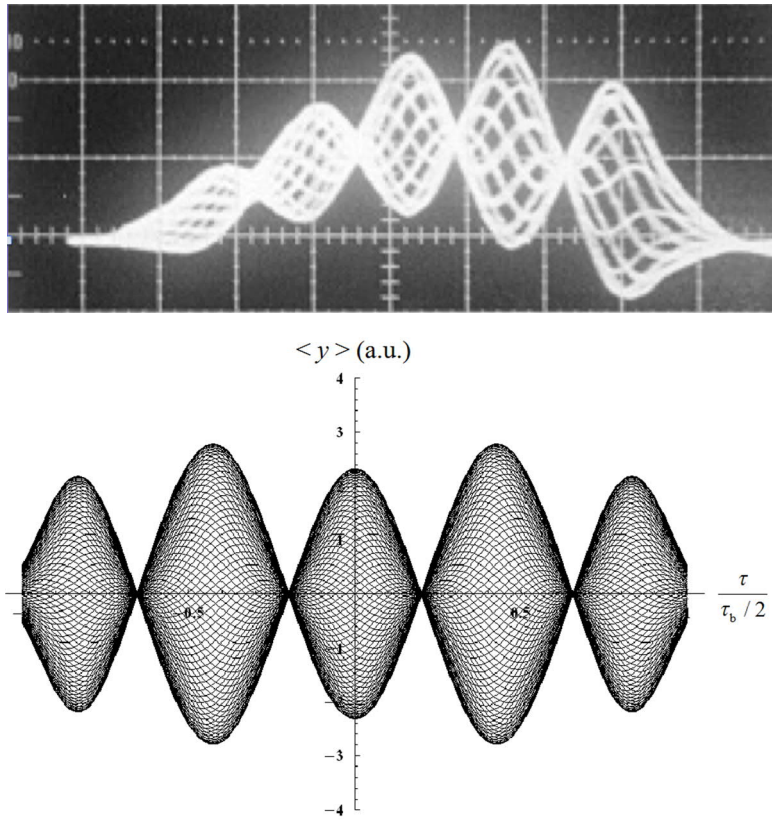

Fig. 10: Top, example of a transverse (slow) head–tail instability observed in the CERN PS at injection (below transition), with several consecutive traces from a pick-up superimposed; a clear ‘standing-wave’ pattern (with four nodes, called ‘mode 4’) can be observed. Bottom, comparison with an analytical prediction (for a bunch passing through the centre of the pick-up).

5 Fast (vertical) single-bunch instability

As the bunch intensity increases, the different head–tail modes can no longer be treated separately. In this regime, the wake fields couple the modes together and a wave pattern travelling along the bunch is created: this is the Transverse Mode-Coupling Instability (TMCI). A simple formula can be obtained from five seemingly diverse formalisms (in the absence of space charge and transverse feedback), assuming a broadband impedance and the long-bunch regime (two assumptions which are discussed below): (i) the coasting-beam approach with peak values, (ii) fast blow-up, (iii) beam break-up, (iv) post-head–tail, and (v) TMCI [1]. An example of a (simulated) TMCI for the case of the CERN Super Proton Synchrotron (SPS), assuming a broadband impedance and without taking into account the effects of both space charge and transverse damper, is shown in Fig. 11 (versus the bunch current I_b) [9], where the HEADTAIL tracking code [10] and MOSES calculations [11] are compared. Good agreement was observed between the two codes, which both showed a coupling between the (azimuthal) modes −2 and −3. Figure 11 (bottom) shows the imaginary part of the normalized tune shift, which is equal to

$$\frac{T_s}{2\pi\tau_{\text{instab}}}, \tag{8}$$

where T_s is the synchrotron period and τ_{instab} the rise time of the instability. Figure 11 (top) shows why the TMCI is more critical close to the transition energy, as the various azimuthal modes are spaced by the synchrotron tune Q_s, which tends to zero as the transition is approached.

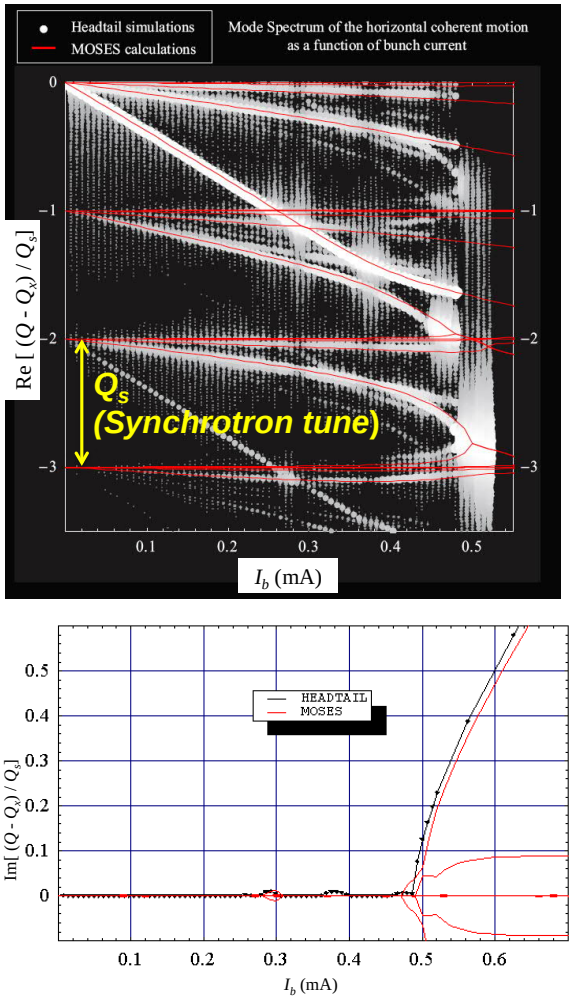

Fig. 11: Example of a simulated TMCI in the CERN SPS [9]: (top) real part and (bottom) imaginary part of the normalized tune shift versus the bunch current.

An example of a broadband impedance (i.e., a resonator impedance with a quality factor $Q = 1$), the first assumption discussed above, is shown in Fig. 12 for a case similar to that of the CERN SPS. The threshold for the TMCI long-bunch regime, the second assumption discussed above, is shown in Fig. 13: the long-bunch regime corresponds to the case where the product of the bunch length and the broadband resonance frequency f_r is much greater than ½.

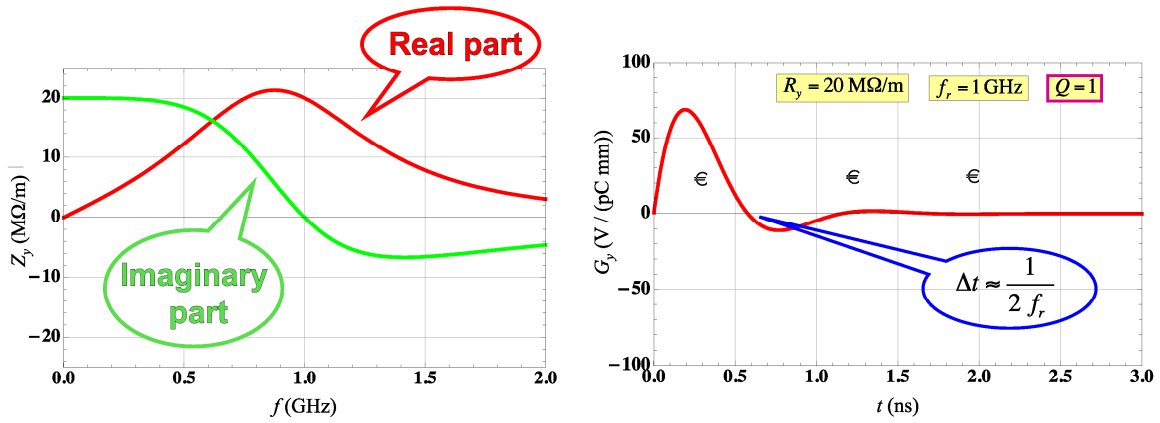

Fig. 12: Example of a (vertical) broadband impedance for a case similar to that of the CERN SPS: (left) real and imaginary parts versus frequency, (right) the corresponding wake function (or Green function) versus time.

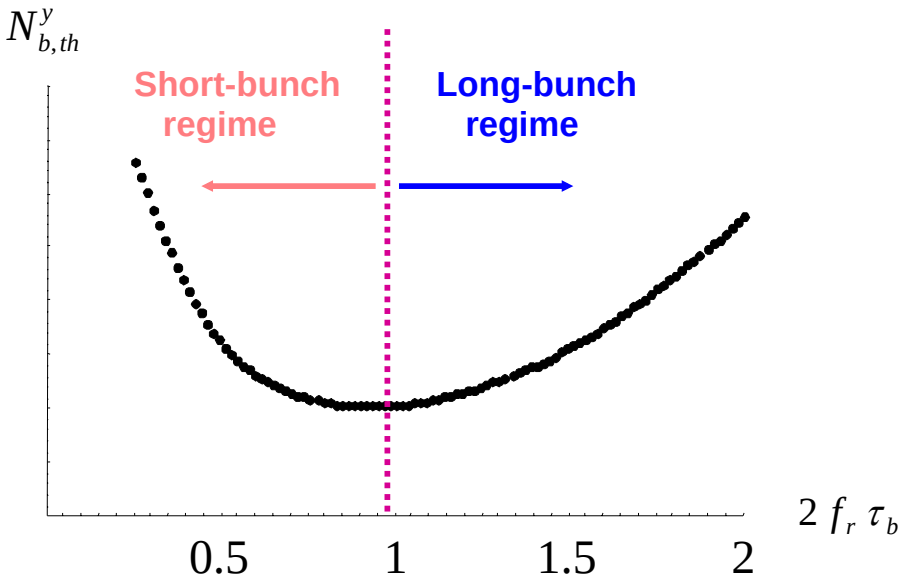

Fig. 13: TMCI threshold (number of particles per bunch) versus the product of the total (4σ) bunch length and the broadband resonance frequency.

Assuming that the two assumptions above are valid, a simple formula giving the threshold number of particles per bunch can be written as follows:

$$N_{b,th}^{y} \propto \frac{f_r}{|Z_y|}\,|\eta|\,Q_y\,\varepsilon_L\left(1+\frac{f_{\xi_y}}{f_r}\right) \tag{9}$$

- Increase the chromatic frequency - Chromaticity jump if transition has to be crossed

Increase the beam longitudinal emittance (when possible)

Try to decrease the impedance and/or increase the resonance frequency => Impedance reduction campaign

Change the optics to increase the betatron tune (decrease the beta function at critical impedances) and/or go further away from transition => New optics needed

where various means to increase the intensity threshold are also mentioned. Note that there is no dependence on Q_s in Eq. (9): what is important is the distance from transition, expressed through the slip factor. Equation (9) also shows that the TMCI does not disappear at high energy (even though the beam becomes increasingly stiff) but the intensity threshold saturates with the slip factor, as has been checked with the HEADTAIL code [12].

In the CERN PS, even in the presence of a γ_t jump together with a change in the sign of both chromaticities when the transition is crossed, a fast vertical single-bunch instability is observed (with the nTOF bunch) when no longitudinal-emittance blow-up is applied before the transition. An example of such an instability is shown in Fig. 14. The instability was suppressed by increasing the longitudinal emittance [13].

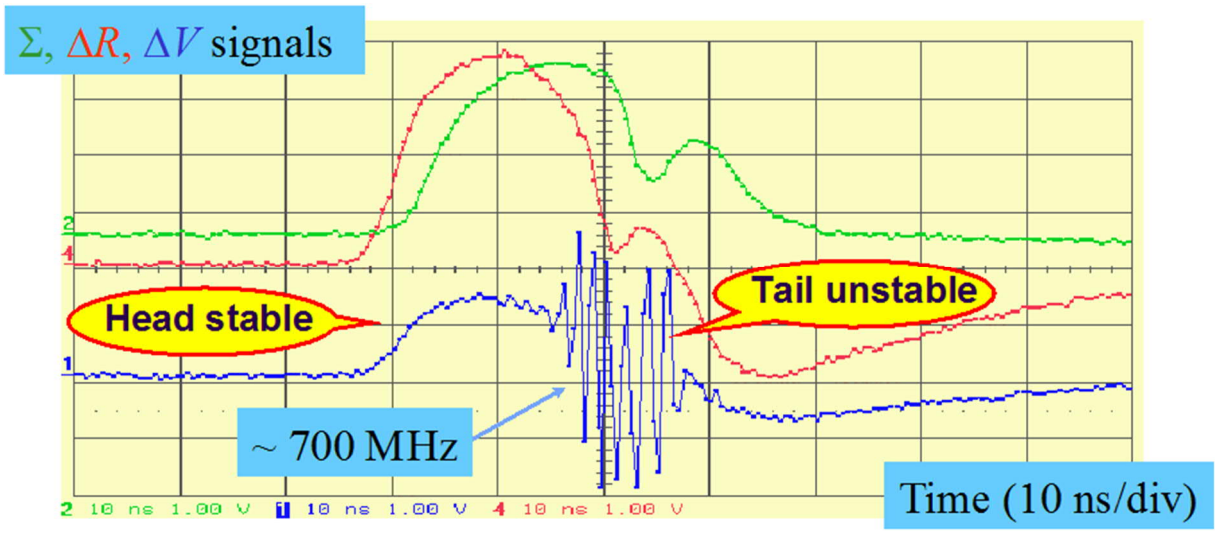

Fig. 14: Single-turn signals from a wideband pick-up in the CERN PS observed in 2000 with an nTOF bunch. From top to bottom: Σ (sum signal), Δ*R* (radial/horizontal signal), and Δ*V* (vertical signal). Time scale: 10 ns/div.

In the CERN SPS, a fast vertical single-bunch instability was first observed when the longitudinal emittance of the bunch was too small, an example of which is shown in Fig. 15 [14]. The instability was first stabilized by increasing the chromaticities, but high values of chromaticities can also have detrimental effects on the beam lifetime (in particular for the nominal multibunch beam in the LHC). In

contrast to the standing-wave pattern observed in the case of the (slow) head–tail instability shown in Fig. 10, this instability exhibited a 'travelling-wave' pattern at low chromaticity (see Fig. 16 (top); this can be seen better in the movie available with the slides for this course). The instability was suppressed at high chromaticity (see Fig. 16 (bottom); the movie shows clearly how a high chromaticity prevents the instability from developing).

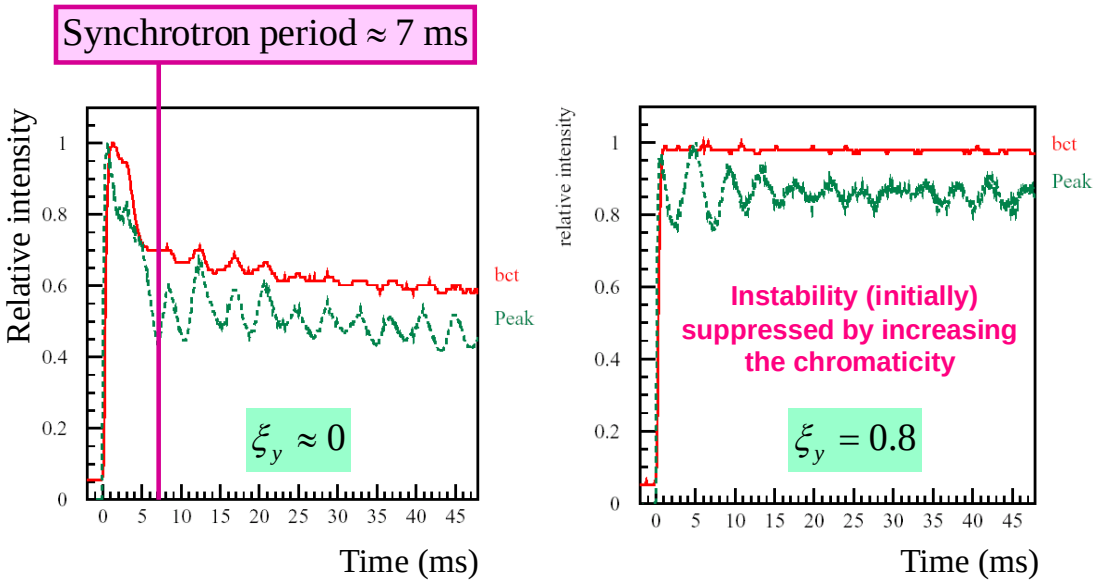

Fig. 15: Normalized bunch intensity (red curve) versus time after injection in the CERN SPS with (left) chromaticity ~0 and (right) chromaticity ~0.8.

Following Eq. (9), the value of γ_t for the SPS has recently been modified to increase the TMCI intensity threshold above the intensities foreseen in future upgrades. For a machine made of simple FODO cells, the following simple estimates of the horizontal dispersion and γ_t can be derived (approximating the machine radius by the bending radius):

$$D_x \approx \frac{\rho}{Q_x^2}, \qquad \gamma_t \approx Q_x . \tag{10}$$

Therefore, if one wants to modify γ_t (i.e., increase or decrease its value), one needs to modify the horizontal tune. This is what has been done in the SPS, where the integer tune was decreased from 26 (in the nominal optics, known as the Q26 optics) to 20 (in the new optics, known as the Q20 optics) [15]. In the case of the Q26 optics, $\gamma_t = 22.8$ and $|\eta| Q_y = 0.62 \times 10^{-3} \times 26.13 \approx 0.0162$ (at SPS injection at 26 GeV/c), while in the case of the Q20 optics, $\gamma_t = 18$ and $|\eta| Q_y = 1.80 \times 10^{-3} \times 20.13 \approx 0.0362$. Therefore, according to Eq. (9), the intensity threshold should be increased by a factor of $0.0362/0.0162 \approx 2.2$. As the TMCI intensity threshold with the Q26 optics was measured to be $\sim 1.7 \times 10^{11}$ p/b [9], the expected intensity threshold with the Q20 optics was $\sim 3.7 \times 10^{11}$ p/b. Measurements performed with the Q20 optics showed good agreement with Eq. (9), as the measured intensity threshold was $\sim 4.5 \times 10^{11}$ p/b, i.e., a gain by a factor of ~2.6 was achieved instead of the ~2.2 foreseen, as can be seen from Fig. 17 [15]. A detailed comparison of measurements and HEADTAIL simulations showed even better agreement, as can be seen from Fig. 18. It can be concluded that with the new Q20 optics, the predicted and measured intensity thresholds are $\sim 4.5 \times 10^{11}$ p/b, i.e., well above the maximum value discussed for future upgrades.

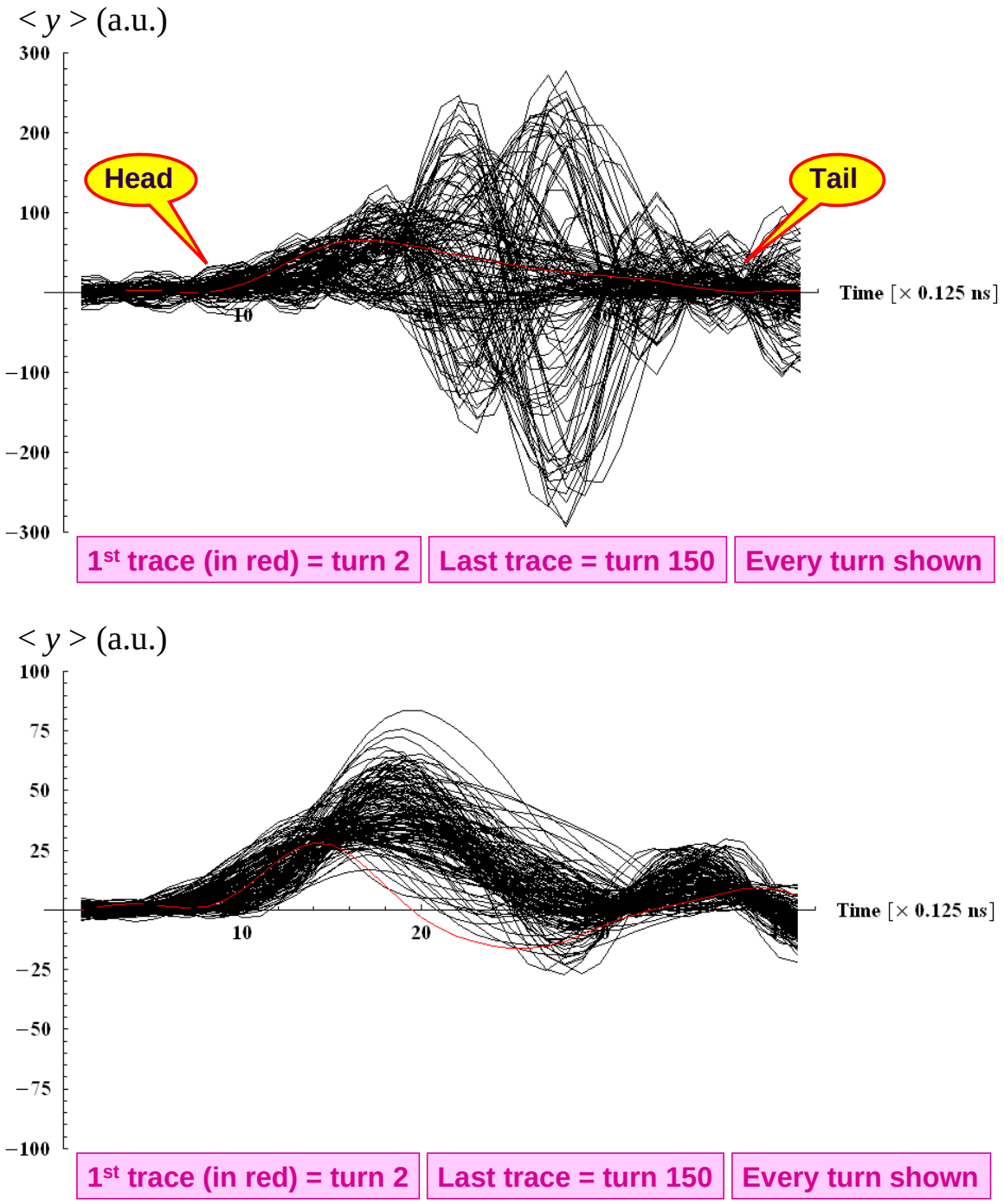

Fig. 16: Top, travelling-wave pattern along the bunch (which can be seen better in the movie available with the slides for this course) during an instability observed at low (~0.14) chromaticity. Bottom, a high chromaticity (~2.04) prevents the instability from developing.

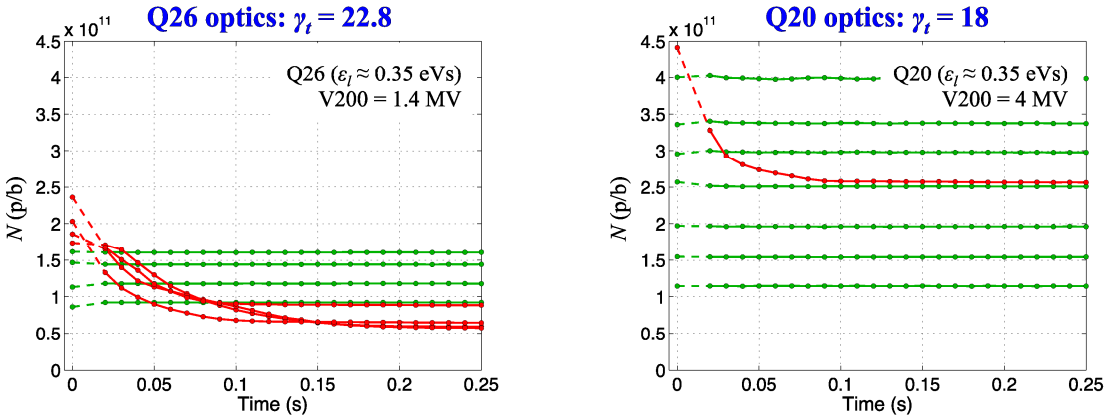

Fig. 17: Number of protons per bunch versus time after injection into the SPS at 26 GeV/*c*: (left) with the old Q26 optics, showing a threshold at ~1.7 × 10^{11} p/b [9], and (right) with the new Q20 optics, showing a threshold at ~4.5 × 10^{11} p/b [15].

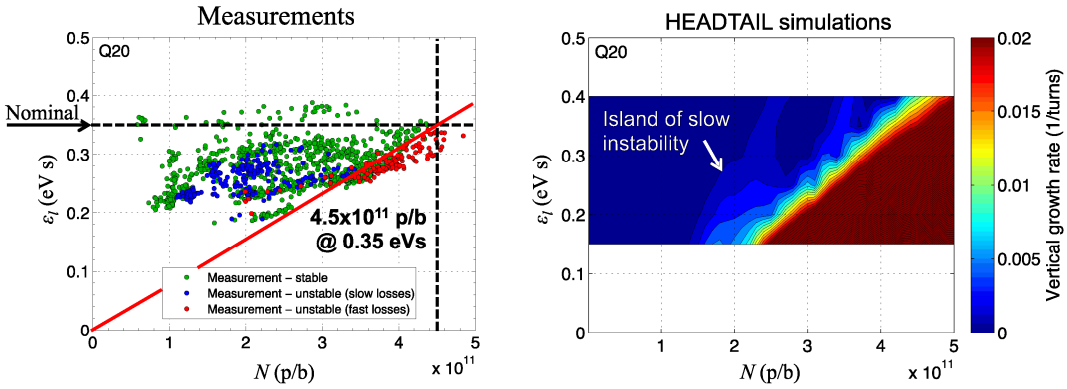

Fig. 18: Detailed comparison between (left) measurements and (right) HEADTAIL simulations of the longitudinal emittance required to reach stability, versus bunch intensity [15].

6 Conclusion

Many intricate beam dynamics effects are observed near the transition energy and when it is crossed. To ensure single-particle longitudinal phase stability, the first thing to be done when the transition is crossed is to shift the synchronous phase from ϕ_s below transition to $\pi - \phi_s$ above transition. Then, to avoid the most critical instability, namely the (slow) head–tail instability of (azimuthal) mode 0, the chromatic frequency should be kept positive, i.e., the signs of the two transverse chromaticities should be changed from negative below transition to positive above transition. Furthermore, above a certain intensity, a TMCI might develop. A simple approximate formula, valid in the presence of a broadband impedance and in the long-bunch regime (the effects of space charge and transverse feedback are still under discussion), shows that the various possible remedies for this are: (i) an impedance reduction campaign; (ii) an increase in the longitudinal emittance (as in the CERN PS); (iii) an increase in the absolute value of the slip factor (as in the SPS) and/or the tune; (iv) an increase in the chromatic frequency (below or above transition); and (v) a 'chromaticity jump' when the transition is crossed, i.e., not only do the signs of the transverse chromaticities need to be changed (because of the head–tail instability) but also the shape could be optimized (because of the possibility of a TMCI).

Furthermore, increasing the absolute value of the slip factor also helps in dealing with the longitudinal mode-coupling instability [16–18] and the fast single-bunch electron cloud instability [12, 15, 19]. Therefore, in most cases a very efficient way to push the performance of a machine near

transition to higher levels is either to go further away from the transition or to cross it as fast as possible (fast compared with the relevant instability rise times).

Finally, as was seen at the beginning of this paper, the operation of a synchrotron under isochronous or quasi-isochronous conditions can be attractive as it (naturally) achieves very short bunches, and for this reason it has been considered in several projects. This requires accurate control of the first high-order component α_1 of the momentum compaction factor (to provide the necessary momentum acceptance, with

$$C(\delta) = C_0\left[1+\alpha_0\,\delta\left(1+\alpha_1\,\delta+\alpha_2\,\delta^2+\ldots\right)\right], \tag{11}$$

where C_0 is the on-momentum circumference and $\delta = \Delta p/p$), as well as effective ways to damp all the collective instabilities.

References

[1] E. Métral and D. Möhl, Transition crossing, in Fifty years of the CERN proton synchrotron, Eds. S. Gilardoni and D. Manglunki, Vol. 1, CERN-2011-004 (2011), p. 59. http://dx.doi.org/10.5170/CERN-2011-004

[2] L. Rinolfi, Longitudinal beam dynamics (application to synchrotron), CERN/PS 2000-008 (LP) (2000).

[3] G. Plass (Ed.), Design study of a facility for experiments with low energy antiprotons (LEAR), CERN/PS/DL 80-7 (1980).

[4] K.Y. Ng, *Physics of Intensity Dependent Beam Instabilities* (World Scientific, Singapore, 2006), p. 691.

[5] S. Andriamonje *et al.*, Neutron TOF facility (PS213): technical design report, CERN-INTC-2000-004 (2000).

[6] A. Chao, Beam instabilities in circular machines, these proceedings.

[7] A.W. Chao, *Physics of Collective Beam Instabilities in High Energy Accelerators* (Wiley, New York, 1993).

[8] S. Aumon, High intensity beam issues in the CERN PS, CERN-THESIS-2012-261 (2012).

[9] B. Salvant, Impedance model of the CERN SPS and aspects of LHC single-bunch stability, CERN-THESIS-2010-087 (2010).

[10] G. Rumolo and F. Zimmermann, Practical user guide for HEADTAIL, CERN-SL-Note-2002-036-AP (2002).

[11] Y.H. Chin, User's guide for new MOSES version 2.0: mode-coupling single bunch instability in an electron storage ring, CERN/LEP-TH/88-05 (1988).

[12] G. Rumolo *et al.*, Simulation study on the energy dependence of the TMCI threshold in the CERN-SPS, CERN-AB-2006-075, Proc. EPAC'06, Edinburgh, UK (2006).

[13] S. Hancock and E. Métral, Ghost bunches and blow-up losses with high-intensity beams, PS/RF Note 2002-198 (2002).

[14] G. Arduini, H. Burkhardt, and E. Métral, Observation of a fast single bunch instability on protons in the SPS, CERN AB-Note-2003-093 (MD) (2003).

[15] H. Bartosik, Beam dynamics and optics studies for the LHC injectors upgrade, CERN-THESIS-2013-25 (2013).

[16] F.J. Sacherer, *IEEE Trans. Nucl. Sci.* **NS-24** (1977) 1393. http://dx.doi.org/10.1109/TNS.1977.4328955

[17] K. Ng, Potential-well distortion and mode-mixing instability in proton machines, FERMILAB-FN-630 (1995).

[18] E. Métral, Stability criterion for the longitudinal mode-coupling instability in the presence of both space-charge and resonator impedances, CERN/PS 2001-063 (AE) (2001).

[19] E. Métral, Effect of bunch length, chromaticity and linear coupling on the transverse mode-coupling instability due to electron cloud, CERN/PS 2002-009 (AE) (2002), Proc. ECLOUD02 Workshop, CERN Yellow Report CERN-2002-001, 211 (2002).
http://dx.doi.org/10.5170/CERN-2002-001